the main beam of the H-plane pattern (ϕ=270 deg) and increased radiation in the sidelobe (θ=90 deg), as shown in Fig. 3 (a). The E-plane radiation pattern of the dielectric spherical radome shows slightly lower directivity compared to the antenna just on the mounting plate.

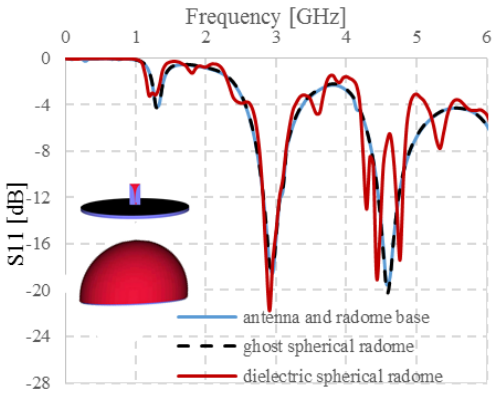

Fig. 2. S_{11} for the antenna on the mounting plate, with the *ghost* spherical radome and the dielectric spherical radome with ε_r=4.2.

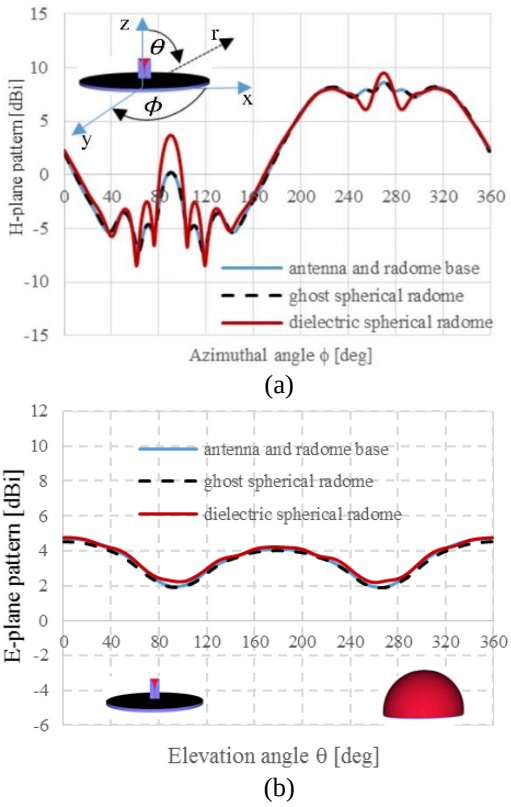

Fig. 3. (a) H-plane pattern and (b) E-plane radiation pattern for antenna on the radome base, with *ghost* spherical radome and the dielectric spherical radome.

III. IMPACT OF DIFFERENT RADOME PROFILES ON ANTENNA PERFORMANCE

In this section, the performance of the Vivaldi antenna installed in several different radomes is analyzed and compared with the case of antenna mounted on the radome base, i.e., without a radome. Illustrative aerodynamic radome profiles are chosen, namely, a spherically blunted cone and two superspheroidal profiles. In all cases, the radome's base radius and length are fixed to be R=2 m and L=2.2 m respectively. In all cases, the half-wave monolithic radome is made of a glass composite of thickness 24.4 mm and dielectric constant ε_r=4.2, which is designed to operate at 3 GHz. Radome losses are neglected. The cone profile radome is blunted by a sphere of radius 0.1 m. The superspheroidal radomes are described by the equation $x^2 + y^2 = \left(\frac{2R}{L}\right)^2 (L^p - z^p)^{2/p}$, where the coordinate z is defined along the axis of the radome, and parameter p defines the particular profile; p=1.449 and p=1.161 give the ogive and superspheroidal profiles of [2] respectively. All simulations were performed with the same meshing and run time parameters given in Section II.

Figure 4 assesses S_{11} in the operating range for the antenna installed in three different airborne radomes. The radome profiles are also given in Fig. 4. Figure 4 shows that reflections from the superspheroidal radomes tend to shift the operating frequency of the antenna and to narrow the antenna's passband. The spherically blunted cone has the least impact on S_{11} in the passband and gives the most similar behavior to the antenna performance without a radome.

Figures 5 (a, b) compares the antenna radiation patterns for the H-plane and E-plane for each radome. Figure 5 (a) shows that the superspheroid with p=1.161 causes the highest deterioration in the main lobe of the H-plane radiation pattern (ϕ=270 deg). The ogive radome (p=1.449) has reduced the directivity of the main beam of antenna (ϕ=270 deg). The spherically blunted radome has the radiation pattern most similar to the antenna with no radome. All radomes cause the slight increase in the side lobe (ϕ=90 deg). Figure 5 (b) shows that in the E-plane, the superspheroid with p=1.161 has significantly increased the directivity of antenna whilst the ogive radome (p=1.449) has decreased the directivity in the E-plane. Again, the spherically blunted radome has the E-plane pattern most similar to the antenna with no radome.

Our analysis of the effect that different superspheroidal radome profiles have on the radiation pattern of the antenna are very different from those in [2] that reported only very minor differences in sidelobes of the antenna radiation. This is, we believe, due to the "decoupled" approach employed in [2].

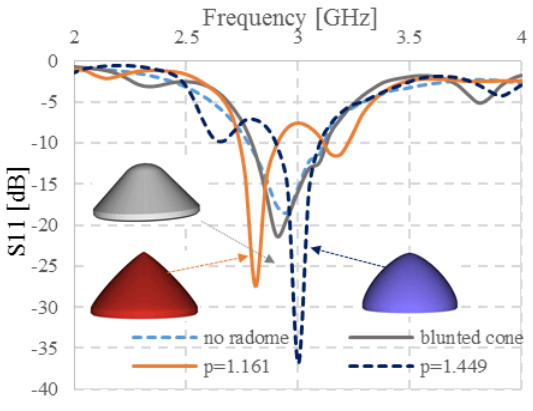

Fig. 4. Comparison of antenna S_{11} parameter in the presence of different radome profiles.

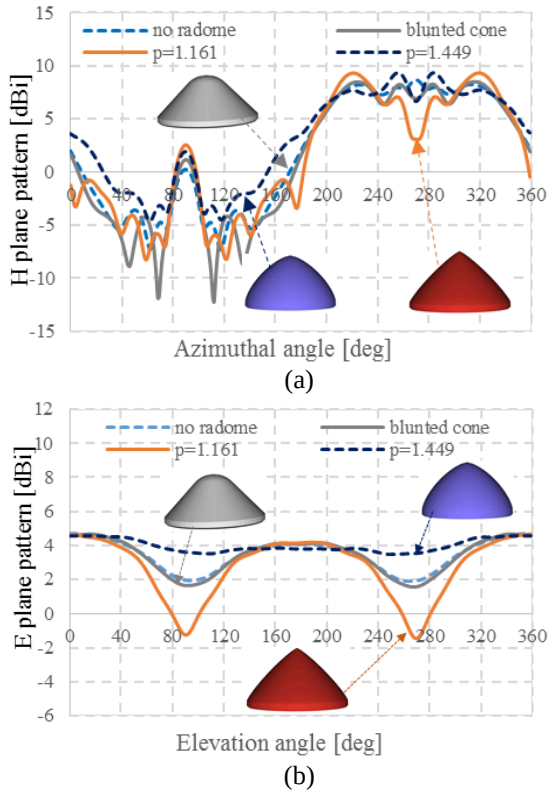

Fig. 5. Comparison of the antenna radiation pattern in the presence of different radomes for: (a) H-plane and (b) E-plane.

IV. CONCLUSION

The paper analyses broadband interactions between antennas installed in airborne radomes in a fully coupled manner by directly sampling both the antenna and the radome geometry using a single numerical method. In order to isolate the effect of the radome, the antenna's performance is first modelled in the presence of just the radome base. Two different superspheroidal radomes and the spherically blunted cone are then introduced and their impact on the antenna's performance assessed. The paper shows that a spherically blunted cone has the least influence on antenna's performance and that superspheroids can significantly change the antennas performance and need to be designed with care.

ACKNOWLEDGMENT

The authors wish to thank Dr. S. Earl and Prof. C. Jones of BAE SYSTEMS for many valuable discussions.

REFERENCES

[1] R. U. Nair and R. M. Jha, "Electromagnetic design and performance analysis of airborne radomes: Trends and perspectives," *IEEE Antennas and Prop. Magazine*, vol. 56, pp. 276-298, 2014.

[2] W.-J. Zhao, L.-W. Li, and Y.-B. Gan, "Efficient analysis of antenna radiation in the presence of airborne dielectric radomes of arbitrary shape," *IEEE Trans. Antennas and Prop*., vol. 53, pp. 442-448, 2005.

[3] P. Sewell, T. M. Benson, C. Christopoulos, D. W. P. Thomas, A. Vukovic, and J. G. Wykes, "Transmission line modeling (TLM) based upon unstructured tetrahedral meshes," *IEEE Trans. Microwave Theory and Tech*., vol. 53, pp. 1919-1928, 2005.

[4] P. Sewell, T. M. Benson, C. Christopoulos, D. W. P. Thomas, A. Vukovic, and J. G. Wykes, "Implicit element clustering for tetrahedral transmission-line modeling (TLM)," *IEEE Trans. Microw. Theory Tech.*, vol. 57, no. 6, pp. 2005-2014, June 2009.

[5] P. Sewell, J. G. Wykes, T. M. Benson, C. Christopoulos, D. W. P. Thomas, and A. Vukovic, "Multi-grid interface in computational electro-magnetics," *Electron. Lett*., vol. 40, pp. 162-163, 2004.

[6] A. E. Yilmaz, Z. Lou, E. Michielssen, and J. M. Jin, "A single boundary implicit and FFT-accelerated time-domain finite element-boundary integral solver," *IEEE Trans. Antennas and Propagat*., vol. 55, pp. 1382-1397, 2007.

[7] J. Shewchuk, Lecture notes on Delaunay Mesh Generation. https://people.eecs.berkeley.edu/~jrs/meshpapers/delnotes.pdf